Please cite this article as "Dogar, A. U. R., Rehman, H. M. U. U., Tafsirojjaman, T., & Iqbal, N. (2020, April). Experimental investigations on inelastic behaviour and modified Gerber joint for double-span steel trapezoidal sheeting. In Structures (Vol. 24, pp. 514-525). Elsevier."

Experimental investigations on inelastic behaviour and modified Gerber joint for double-span steel trapezoidal sheeting

Attiq Ur Rahman Dogar [a], Hafiz Muhammad Ubaid Ur Rehman [b], T. Tafsirojjaman[c,*], Naveed Iqbal[a]

[a] *Department of Civil, Environmental and Natural Resources Engineering, Luleå University of Technology, 971 87 Luleå, Sweden*

[b] *ISISE – Institute for Sustainability and Innovation in Structural Engineering, University of Coimbra, 3004-531 Coimbra, Portugal, Portugal*

[c,*] *School of Civil Engineering and Built Environment, Faculty of Science and Engineering, Queensland University of Technology, 2 George Street, Brisbane, QLD 4000, Australia.*

Email addresses: Corresponding Author: tafsirojjaman@hdr.qut.edu.au (T. Tafsirojjaman*), Tel: +61470244586. attdog-7@student.ltu.se (Attiq Ur Rahman Dogar),uc2017288832@student.uc.pt (Hafiz Muhammad Ubaid Ur Rehman), naveed.iqbal@ltu.se (Naveed Iqbal)

Abstract:

Cold-formed steel trapezoidal profiles provide efficient solutions for roofing and often use the Gerber joint to effectively utilize capacities. The previous design of Gerber joint was sensitive to uneven distribution of loads and accidental loads, which imposed bending moments in the joint and lead to its failure. In this experimental program, the design of Gerber joint has been modified to work as a hinge under service loads and carry moments in accidental conditions. Also, the design of CFS is based on elastic methods that underestimate their capacity, especially for multi-span systems. Full-scale tests were conducted on highly stiffened double-span trapezoidal sheeting profiles with modified Gerber joint to investigate elastic capacity, inelastic behaviour, moment redistribution in the post-elastic phase, ultimate load capacity and feasibility of modified Gerber joint. Comparison of elastic load capacity with EWM and DSM predictions revealed that EWM design predictions were conservative by 30% while DSM predictions were accurate. For multi-span application, residual moment capacity ratios of 0.76 and 0.81 in the post-elastic phase allowed for moment redistribution and increased ultimate load capacity by 7.14% and 8.80% for 0.85 mm and 1 mm thick profiles respectively. Performance of modified Gerber joint to behave as a hinge under service loads and as continuous in the post-elastic phase was also found to be satisfactory. The study concluded that the economy in design and capacity utilization of multi-span CFS profiles can be improved by allowing for moment redistribution and using the modified Gerber joint.

Keywords: Cold-formed steel, trapezoidal sheeting, inelastic behaviour, post-elastic, multi-span sheeting, Gerber joint, direct strength method, moment redistribution.

Nomenclature

CFS	Cold-formed steel
EWM	Effective width method
DSM	Direct strength method
AISI	American Iron and Steel Institute
M^-	Support moment capacity
M^+	Span moment capacity
I_{eff}	Effective moment of inertia
LVDT	Linear variable differential transformers

$\sigma_{cr,l}$	Critical local buckling stress
$\sigma_{cr,d}$	Critical distortional buckling stress
k_{σ}	Plate local buckling factor
ν	Poisson's ratio
t_n	Nominal thickness of the plate
b_n	Nominal width of the plate
$\sigma_{cr,s}$	The elastic critical stress for an intermediate flange stiffener
k_w	Rotational restraint coefficient
A_s	Effective cross-section area of an intermediate flange stiffener
I_s	Moment of inertia of stiffener
b_p	Notional flat width of the plane element
b_s	Stiffener width
$\sigma_{cr,sa}$	The elastic critical stress for a single web stiffener
k_f	Partial rotation restraint of the stiffened web by flanges
A_{sa}	Effective cross-section area of an intermediate web stiffener
$\sigma_{cr,d,\ web}$	Critical distortional buckling stress for web
$\sigma_{cr,d,\ flange}$	Critical distortional buckling stress for flange
$\sigma_{cr,d,\ mod}$	The modified elastic critical stress for stiffeners
GJ	Gerber joint
GM	Midspan with Gerber joint
MS	Midspan
W_{eff}	Effective section modulus
M_d^-	Designed support moment capacity

$M_{cr\ell}$	Critical elastic local buckling moment
M_{crd}	Distortional buckling moment
M_{cre}	Global (lateral-torsional) buckling moment
$M_{n\ell}$	Nominal flexural strength for local buckling
M_{nd}	Nominal flexural strength for distortional buckling
M_{ne}	Nominal flexural strength for yielding and global (lateral-torsional) buckling
Φ	LRFD Resistance factor
M_n	Nominal flexural strength

1. Introduction

Use of lightweight cold-formed steel (CFS) as structural members is gaining popularity over other construction materials i.e. concrete, timber and masonry due to low weight to strength ratio, economy in production, ease of transportation and fabrication. Among these CFS members, corrugated trapezoidal sheeting is used as roofing and can either be used as a composite slab or as a single insulated or non-insulated profile.

High width to thickness ratio of CFS sections increases their sensitivity to instabilities i.e. local, distortional, global or interactive buckling modes and reduces their capacity. A significant amount of research has been carried out on complex buckling modes of CFS members [1,2] and interaction between these buckling modes [3–5].To reduce their susceptibility to buckling, edge and intermediate stiffeners are provided to decrease buckling length of individual plate elements and provide a continuous restraint to these elements. A detailed Finite Element study on the flexural behaviour of CFS Z-sections by Haidarali and Nethercot [6] demonstrated the significant effect of size and position of edge and intermediate stiffeners on buckling modes and bending capacity. A similar result was concluded by Franco and Batista [7] for stiffened trapezoidal sheeting profiles and they proposed trapezoidal-shaped intermediate stiffeners in both webs and flanges for improved buckling behaviour. The strength prediction of CFS members is based on elastic methods i.e. Effective Width Method (EWM) and Direct Strength Method (DSM). EWM is a basic design method of European [8,9] and American AISI specifications [10] for the design of CFS members and follows a traditional philosophy of reduced effective cross-section. For complex cross-sectional shapes with lips and stiffeners, computation of effective cross-section and capacity becomes complex and inaccurate. This computational effort and inaccuracy for complex sections can be significantly reduced by DSM. DSM was initially introduced in 2004 as commentary [11] to AISI 2002 specifications [10] and has been recently codified as a part of AISI 2016 specifications[12]. Unlike EWM, DSM is a semi-analytical approach and considers gross section properties. EWM is appropriate for many CFS profiles, but observed failure modes and failure loads for complex profiles with edge and intermediate stiffeners did not agree well with EWM predictions as reported by Schafer [13]. Therefore, a semi-analytical finite strip solution was developed which provides better predictions for CFS sections as compared to EWM [14].

While the design is based on elastic methods, Yener and Pekoz [15] demonstrated that CFS sections possess significant inelastic reserve capacity and can carry higher loads due to re-distribution of yielding in the cross-section. Tests carried out by Reck et al. [16] on hat sections exhibited that ultimate strain can be three times higher than yield strain. Maduliat et al. [17] compared the experimental capacities of channel sections with design specifications [8-10] and proved the conservative nature of these specifications. Tests conducted by Laím et al. [18] showed that experimental moment capacity was 27% higher than European recommendations [8,9].

Also, elastic design methods predict capacity based on the elastic capacity of single-span CFS sections, which yields uneconomical results for multi-span applications. Studies [19-21] have shown that the CFS section over internal support can rotate significantly in the post-elastic phase under the reduced level of moment resistance (Figure 1a) as compared to hot-rolled sections which can sustain their yield moment resistance over considerable rotations(Figure 1b). This reduced level of moment resistance in CFS sections redistributes moments and ideal re-distribution is achieved when the section in mid-span utilizes its elastic capacity. This concept of post-elastic strength utilization due to moment redistribution in multi-span CFS profiles was first introduced in 1973 by Unger [22]. Based on experimental tests on shallow decking profiles, he proposed that the section over internal support can be replaced by a plastic hinge with reduced elastic moment resistance. This increase in capacity due to redistribution of moments in shallow decking profiles was also demonstrated through experimental tests on continuous deck profiles by Leach [23] and Luure & Crisinel [24]. Test results of Leach [23] showed that two-span systems can sustain loads up-to 56% higher than elastic design predictions. This procedure of replacing the section over internal support by a plastic hinge with reduced resistance is widely used by deck manufacturers and is also a part of CIRIA technical note [25]. Davies [26] developed a finite element model to analyze previous experimental results and proposed a quasi-elastic design procedure that utilizes reduced elastic moment resistance. Based on tests on moment redistribution in deck profiles, Lawson and Popo-Ola [19] proposed an approximate relation to derive the load-carrying capacity of two-span decking. Studies of Liu et al. [20] derived a method for sigma sections and concluded that load carrying capacity for multi-span profiles can be 26% higher than predictions by elastic methods. A similar method was derived by Hui et al. [21] for Z and channel sections.

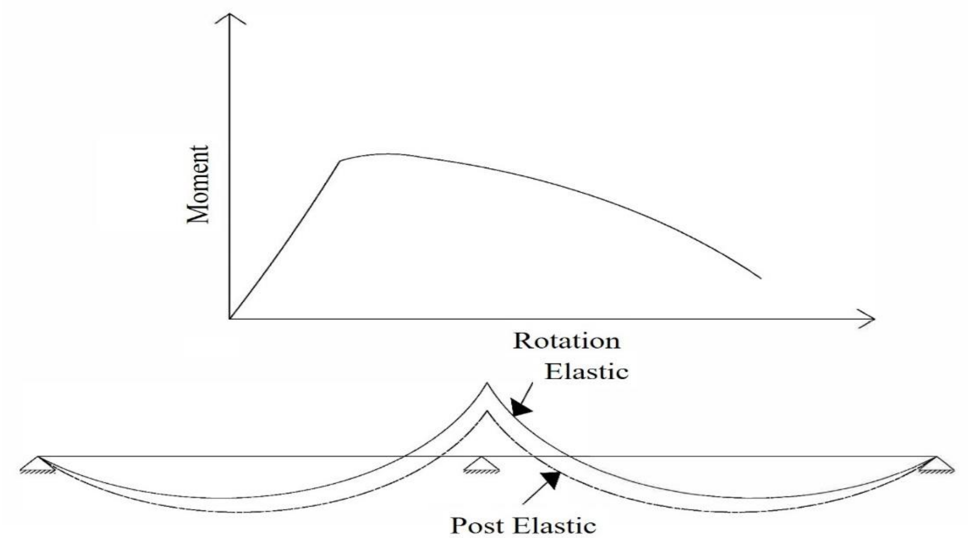

(a)

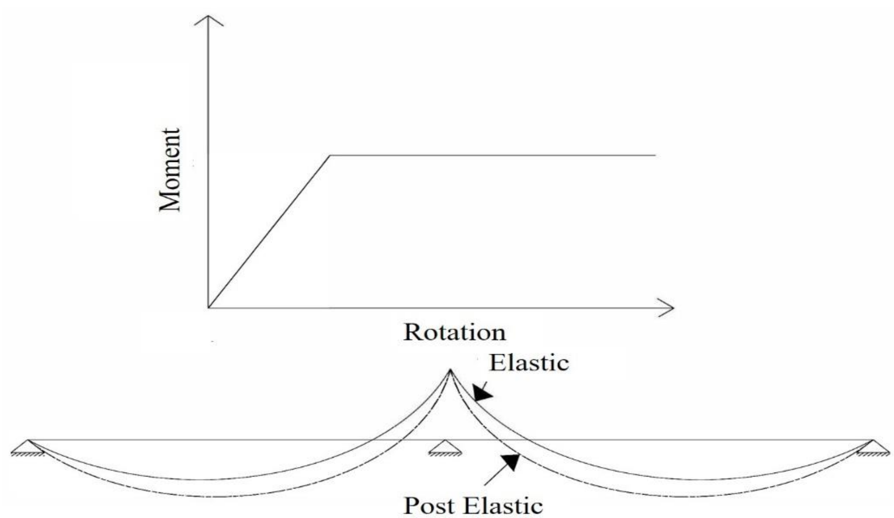

(b)

Figure 1: Moment rotation relationship and moment redistribution in post-elastic phase (a) Cold-formed profiles (b) Hot-rolled profiles

While most of the reported studies on failure modes, inelastic behaviour and load-carrying capacity of multi-span CFS profiles are focused on purlins and un-stiffened shallow deck profiles, there is little information available on third generation stiffened trapezoidal sheeting profiles. These sheeting profiles are used as non-composite roofs and employ a special cantilever drop-in system known as Gerber joint. The design of this Gerber joint has been modified in this study so that it could carry bending moments in the post-elastic phase, explained in section 2. Little to no information is available on Gerber joint and this investigation is the first study on behaviour of the modified Gerber joint. Full-scale experiments were conducted at the Luleå University of Technology to study elastic moment capacity, inelastic behaviour, failure modes of trapezoidal sheeting profile, moment redistribution in the post-elastic phase, ultimate load capacity and to investigate the feasibility of modified Gerber Joint. In this research program, moment capacities and failure modes have been compared with the Eurocode [8,9] and DSM [12] predictions and conclusions have been drawn regarding their accuracy. For the investigation of Gerber Joint, two different test configurations were used and recommendations for modified Gerber joint and moment redistribution have been made by comparing the results of these two configurations. It has been concluded that consideration of inelastic capacity, moment redistribution and utilization of modified Gerber joint in multi-span systems can yield economical design solutions for roofs and purlins.

2. Cantilever Drop-in System (Gerber Joint):

Gerber joint also known as suspended cantilever drop-in system was introduced in 1866 for bridge engineering and was gradually adopted in architectural engineering [27]. This joint has recently found its application in multi-span CFS roofing systems where a profile in the exterior span is made continuous over the internal support up-to a specific distance in the internal span. At this cantilever point in the internal span, the second profile is connected through a shear connection so that the joint resist shear only.

Due to this internal pin, bending moments are optimally distributed allowing for effective utilization of span and support moment capacities [27]. Consider a double span beam with length L, if the profiles in both spans are connected separately at the internal support (Figure 2a), each span will act as a simply supported beam with the maximum bending moment in mid-span i.e. $wl^2/8$. If the beam is continuous (Figure 2b), bending moments are maximum at internal support i.e. $wl^2/8$. However, when one profile from external span is continued over the internal support and connected to the second profile at a pre-defined distance of 0.17xL from internal support (Figure 2c), applied moments in span and support are lowest compared to previous two cases i.e. $wl^2/12$, leading to efficient utilization of span and support moment capacities.

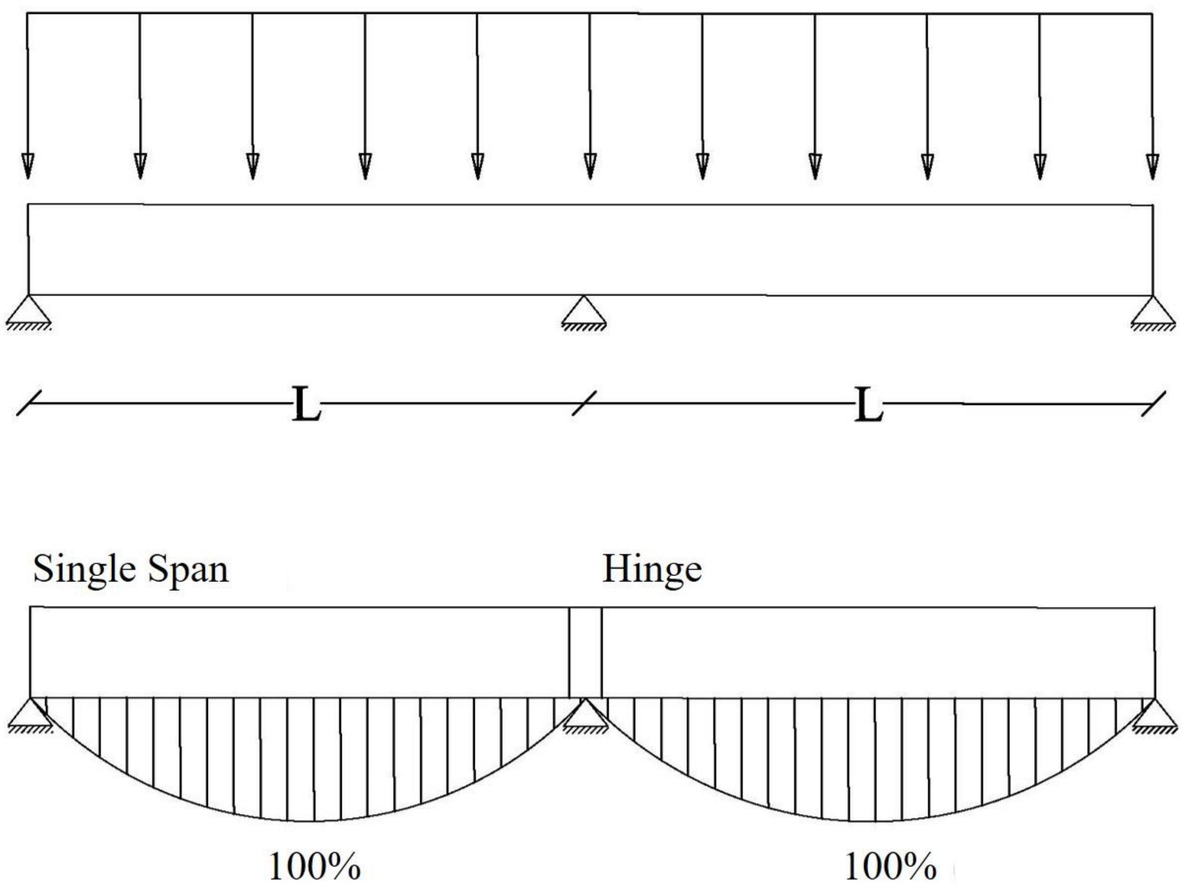

(a)

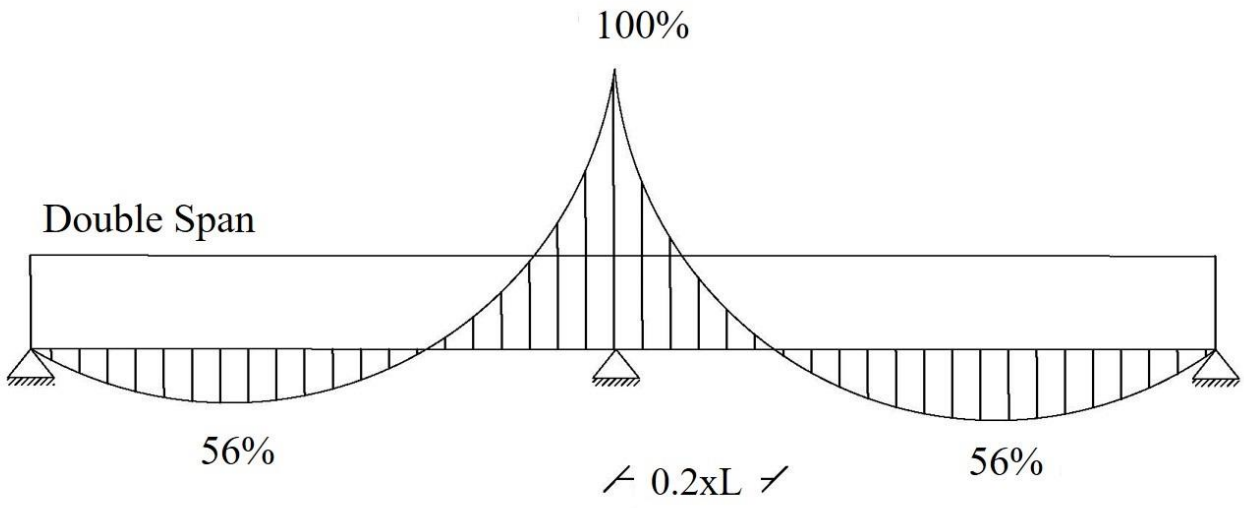

(b)

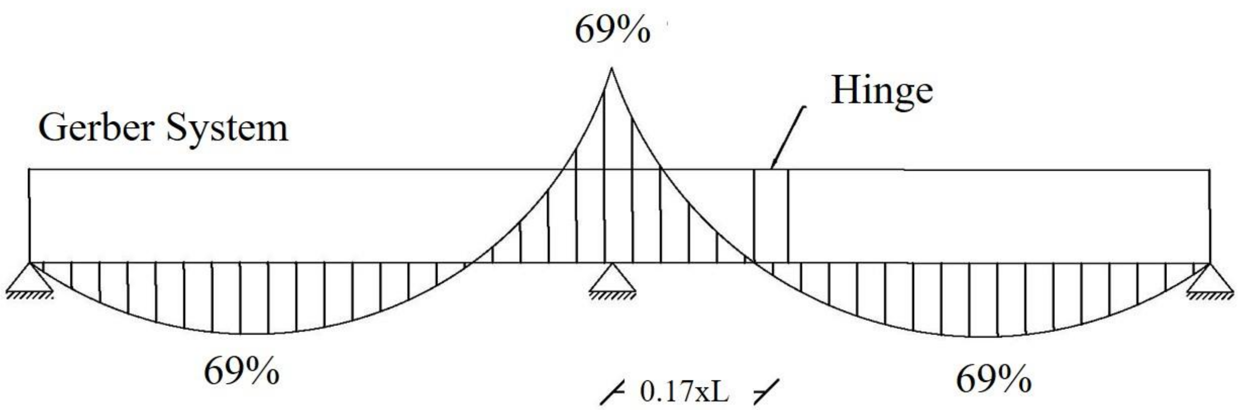

(c)

Figure 2 Distribution of bending moments (a) hinges at support (b) continuous beam (c) Gerber hinge

2.1. Gerber Joint for trapezoidal sheeting profile:

Gerber joint for steel trapezoidal sheeting profile was previously made by overlapping two profiles with an overlap length of 200 mm and screws in the center of overlap (Figure 3a). Previous investigations [28–31] on the behaviour of this joint revealed its inadequacy under the uneven distribution of loads or accidental conditions that engender bending moments in the joint. They demonstrated that the joint does have some rotational stiffness which is insufficient to carry accidental moments. Therefore, the design of the Gerber joint has been modified in this research study by increasing the overlap length from 200 mm to 500 mm and moving the screws towards the right end of overlap (Figure 3b). A single cross-section in this modified design now has a total of 6 screws, 2 in the top flange and 4 in the web. L_s indicates the distance of the center of the Gerber joint from internal support.

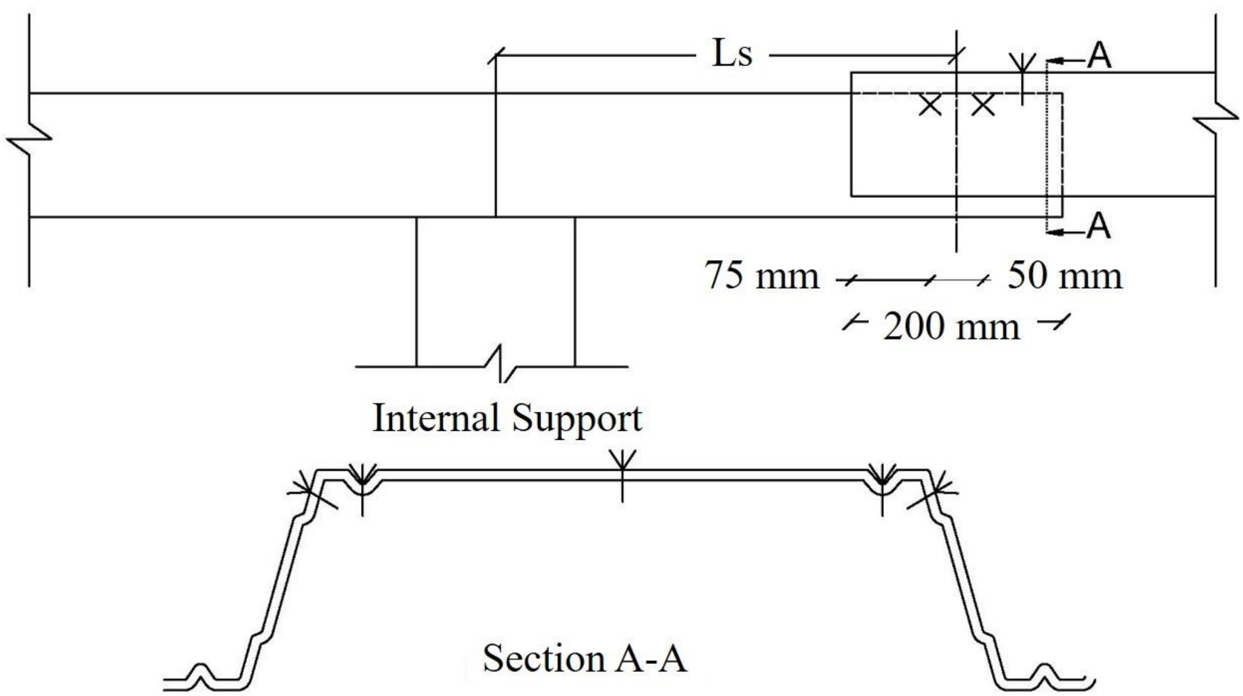

(a)

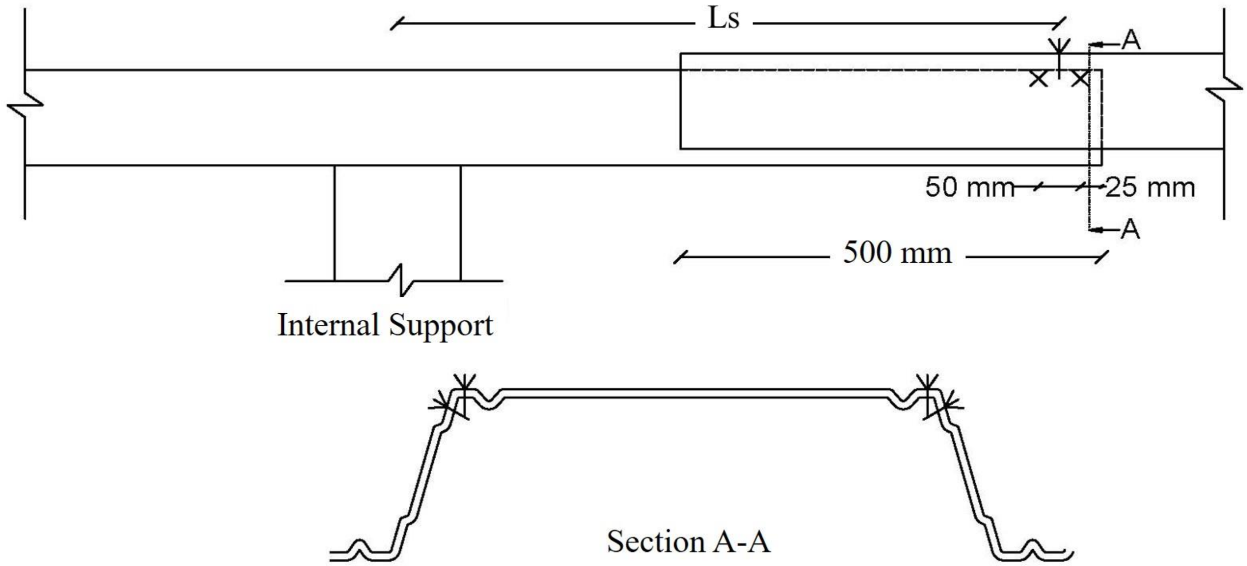

(b)

Figure 3: Design of Gerber joint (a) previous (b) modified

The basic intention behind the modification of Gerber joint is that it should behave as a hinge under service conditions and as a continuous joint under accidental loads i.e. post-elastic phase. This ensures optimal utilization of capacity in service conditions and the safety of joints in the post-elastic phase. To understand the mechanism of modified joint design, consider a uniformly loaded double-span beam with a modified Gerber joint (Figure 4a). During the elastic phase, section over internal support is fully stiff and both the profiles rotate in opposite directions around the screws and gap at the free end opens up (Figure 4b), making the joint a hinge. As buckling of section over internal support initiates, it loses stiffness and the gap between profiles closes and the modified joint starts acting as continuous due to a combination of overlap and screws (Figure 4c). This design assumption has been verified by measuring the gap between profiles during the elastic and post-elastic phase. Two different test setups were used in this study with different overlap lengths replicating the modified Gerber joint and previous Gerber joint. The collapse mechanism of both test setups was also compared to verify the design assumption. In the first test setup replicating modified Gerber joint, longer overlap length provides continuity in the post-elastic phase allowing for moment redistribution and collapse mechanism is formed when elastic bending capacity of the section in mid-span is reached. Conversely, joint in a second test setup with shorter overlap was insufficient to transfer any moments in the post-elastic phase, therefore, the collapse mechanism is supposed to be either by failure of the region between internal support and Gerber joint or by failure of Gerber joint itself.

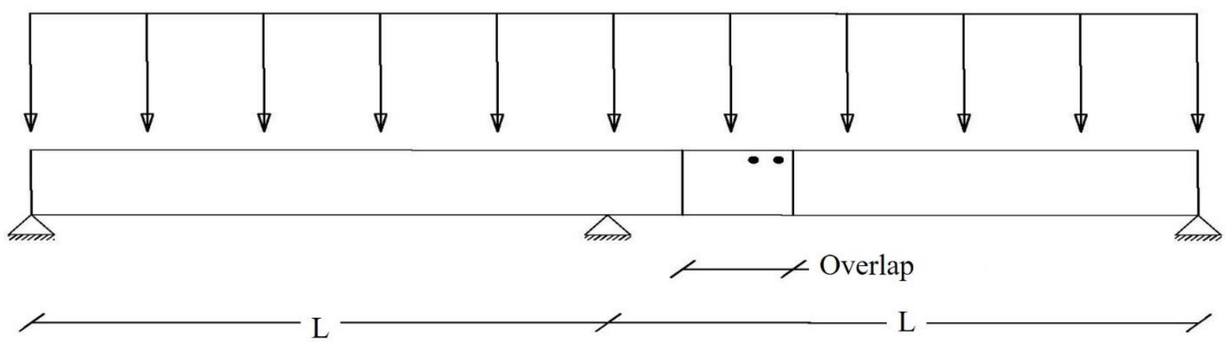

(a)

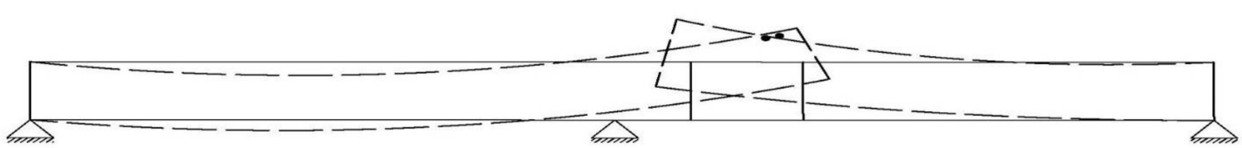

(b)

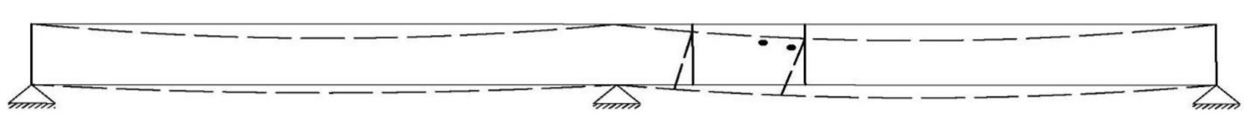

(c)

Figure 4: Behaviour of modified Gerber joint (a) uniformly loaded span (b) elastic phase (c) post-elastic phase

3. Experimental Tests:

3.1. Test specimens:

Full-scale experiments were conducted at the Luleå University of Technology on third-generation steel trapezoidal sheeting profiles with both longitudinal and transverse stiffeners manufactured by Lindab International. The profile is made of S420 grade steel with zinc coating. Two class 4 sections with profile thicknesses of 0.85 mm and 1 mm were tested and cross-sectional dimensions of the centerline of profiles are shown in Figure 5. The test specimen was made of two steel profiles overlapped at the bottom flange making a total width of 1600 mm (Figure 6a (Section A-A)). The bottom flange of each profile is 75 mm wide with one intermediate stiffener and the top flange is 540 mm wide with two intermediate stiffeners. Manufacturer provided steel core thicknesses, effective moment of inertias and single-span negative (M^-) and positive (M^+) moment capacities of single section profiles (800 mm) are given in Table 1. Manufacturer recommended yield strength and modulus of elasticity i.e. 420 MPa and 210 GPa have been used for calculations. Self-drilling stainless steel screws of 6.3 mm diameter and 8.5 kN shear resistance were used for each connection. Since the profile is un-symmetric about the bending axis, therefore, negative and positive moment capacities are different depending on flange in compression.

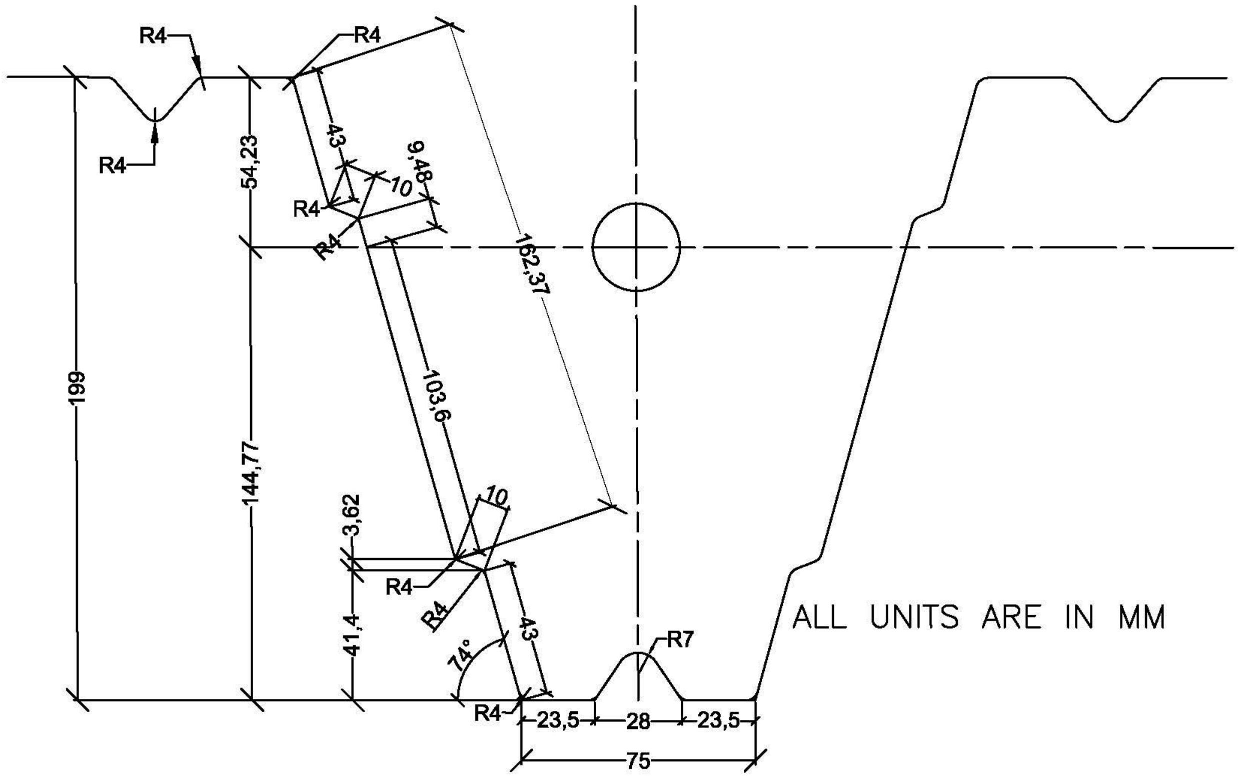

Figure 5: Centerline dimensions of trapezoidal sheeting profile

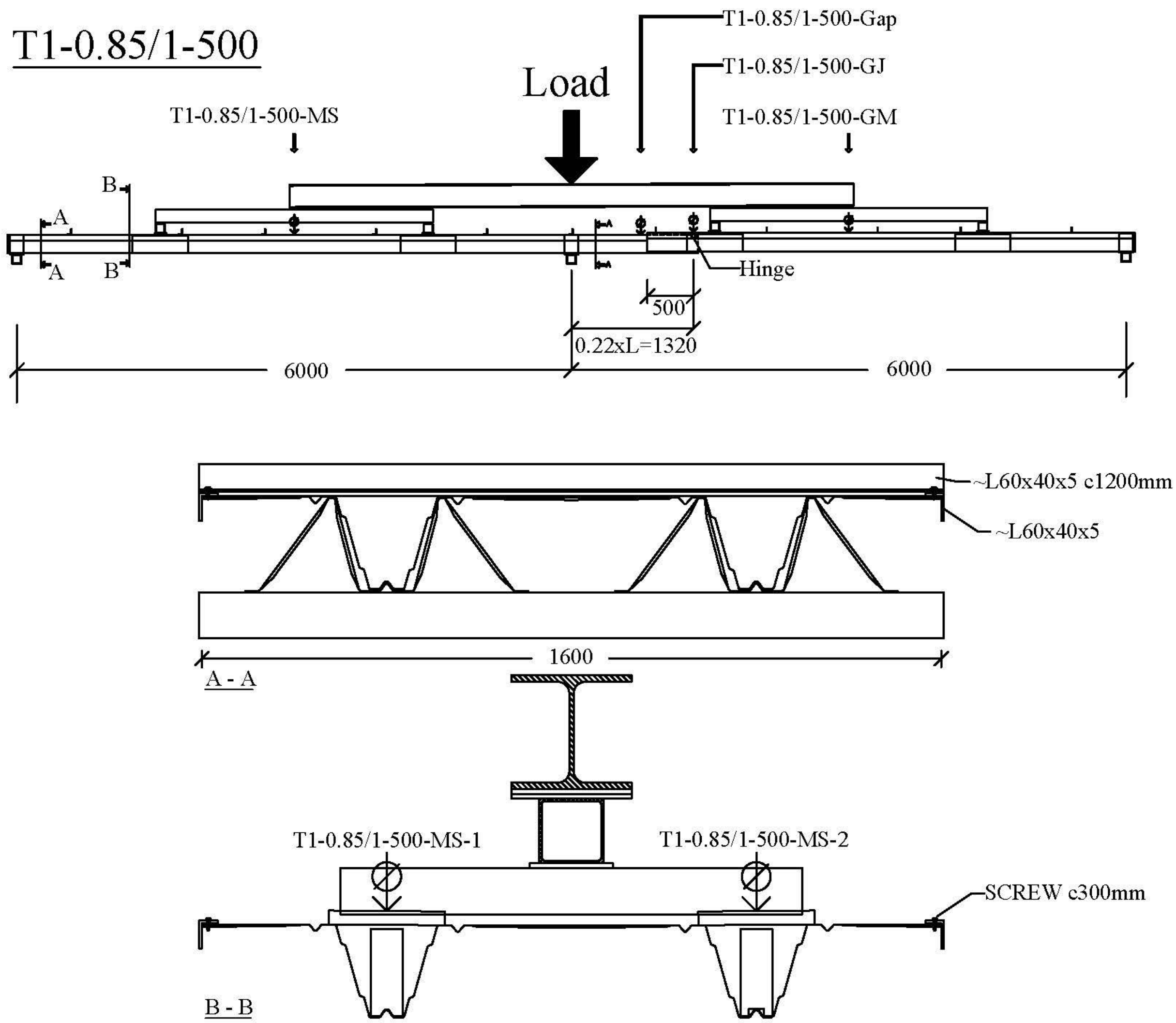
T1-0.85/1-500
T1-0.85/1-500-Gap
T1-0.85/1-500-GJ
Load
T1-0.85/1-500-MS
T1-0.85/1-500-GM
B
A
A
B
Hinge
500
0.22xL=1320
6000
6000
~L60x40x5 c1200mm
~L60x40x5
1600
A - A
T1-0.85/1-500-MS-1
T1-0.85/1-500-MS-2
SCREW c300mm
B - B

(a)

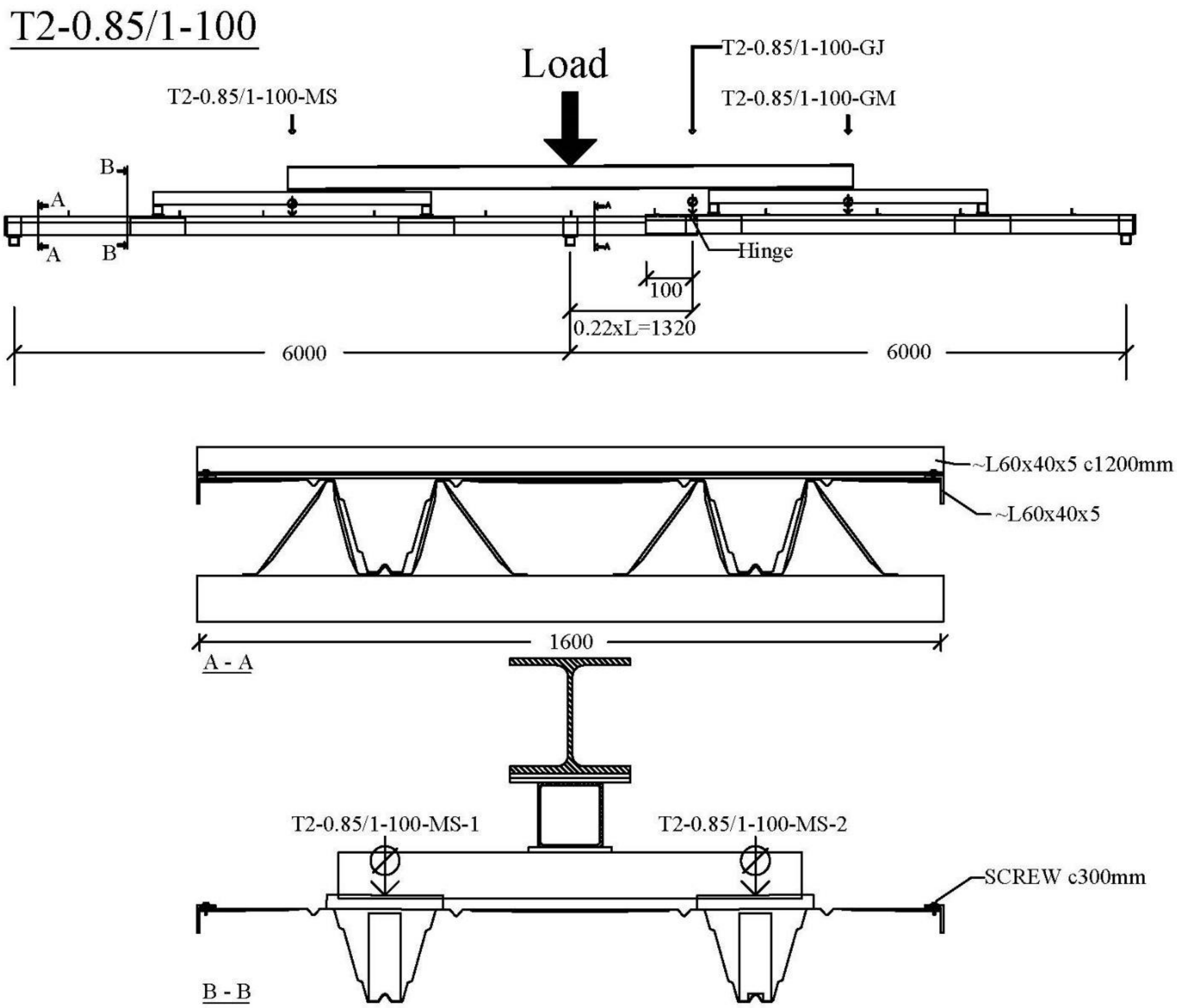
T2-0.85/1-100
Load
T2-0.85/1-100-MS
T2-0.85/1-100-GJ
T2-0.85/1-100-GM
Hinge
100
0.22xL=1320
6000
6000
A
A
B
B
~L60x40x5 c1200mm
~L60x40x5
1600
A - A
T2-0.85/1-100-MS-1
T2-0.85/1-100-MS-2
SCREW c300mm
B - B

(b)

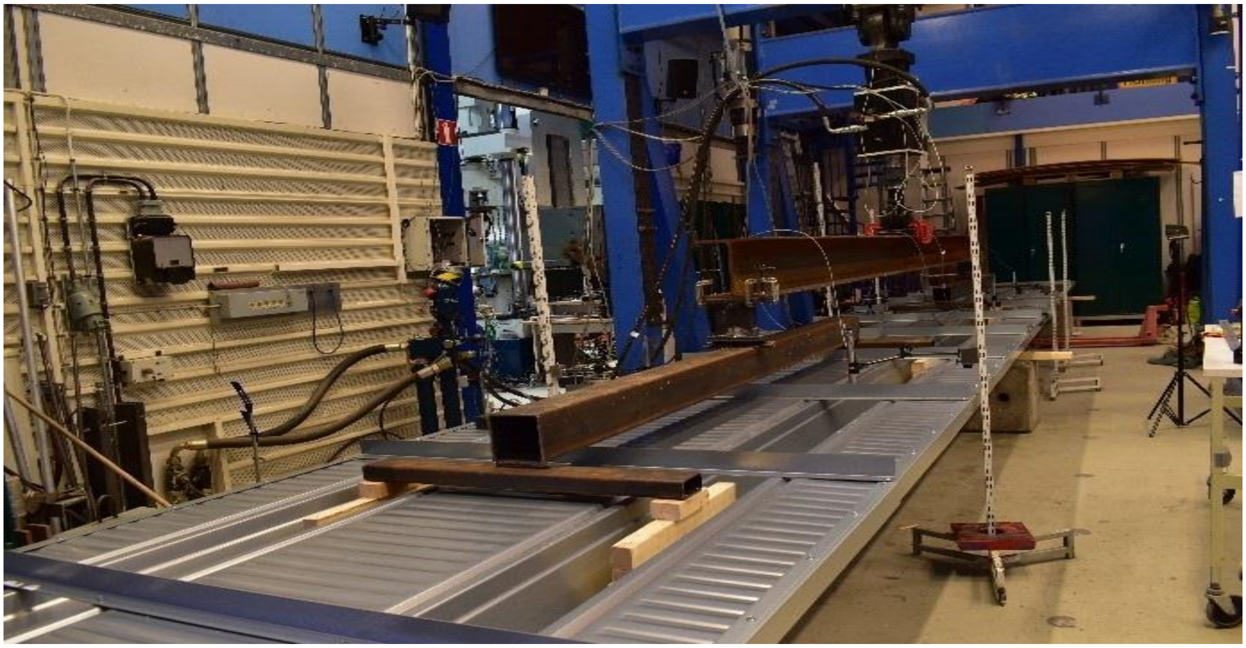

(c)

(d)

Figure 6: Experimental setup (a) Test setup-1 schematic (b) Test setup-2 schematic (c) and (d) setup views

Table 1: Manufacturer recommended section properties and tested single-span capacities of trapezoidal sheeting

Profile thickness (mm)	Core Thickness (mm)	I_{eff} ($x10^6$ mm^4)	Single span moment capacity (kN-m)	
			Support (M^-)	Span (M^+)
0.85	0.782	3.568	10.608	7.736
1	0.940	4.328	14.664	10.888

3.2. Test Setup:

Full-scale experiments were conducted on a double-span profile with the length of each span (L) 6 m subjected to four-point loading (Figure 6). Supports were made by mounting 150mm long support cleats on timber boards using self-drilling screws. To prevent distortion of the web under concentrated loads, support cleats were connected to the top flange only, providing a gap between the bottom of profile and support cleat. Side overlap at bottom flange was made by joining both flanges using self-drilling screws with c/c longitudinal spacing of 500mm in span and 250mm near the internal support to account for negative bending. In order to prevent the section from distortion, EN 1993-1-3 [8] Annex A.2.1 recommends the use of transverse ties. A combination of longitudinal and transverse ties was used with angle sections L60x40x5.

For each profile thickness, two different test configurations with varying overlap length for Gerber joint were used, named as (1) Test Setup-1 and (2) Test Setup-2. Test setups are designated as test setup–profile thickness–overlap length (Table 2). In each test setup, profile from one span was made continuous over the internal support like a cantilever up-to an effective distance of 0.22xL+50 mm (optimum location of modified Gerber hinge) making a total length of 7.37 m. The location of Gerber joint was changed from 0.17xL to 0.22xL due to different spans and support moment capacities. The second profile was placed over this cantilever with an overlap length of 500mm in test setup-1 and 100mm in test setup-2. The placement of screws was the same as in Figure 3b.

Table 2**:** Test setup summary

Test Setup	Gerber Joint	Overlap Length (mm)	Profile Thickness (mm)	Test Setup Designation
1	Modified	500	0.85	T1-0.85-500
		500	1	T1-1-500
2	Previous	100	0.85	T2-0.85-100
		100	1	T2-1-100

Test setup-1 is intended to be used in the future in the field and the reason for testing was to ensure if it can carry accidental moments in the post-elastic range. The assumption that the joint behaves as a hinge under service loads (elastic phase) and as continuous (post-elastic phase) was verified by measuring the gap at end of overlap. Since in the elastic range, the section at internal support is stiff, therefore, this gap between profiles opens up. Due to the loss of stiffness in the post-elastic phase, the gap closes and profiles overlap to resist moments.

The load was applied through a hydraulic jack on the I-section beam (Figure 6) with a stroke of 2mm/min. Each end of the I-beam was supported on hollow steel sections which then transferred the load onto timber blocks. Two 75 mm long blocks then transferred the load onto the bottom flange of the sheeting profile. Deflections of the top flange were measured using LVDTs (Figure 6a and 6b). LVDTs are designated as test setup–profile thickness–overlap length-LVDT location (Table 3). MS indicates LVDT in midspan, Gap is for measurement of the gap, GJ is the location of screws of Gerber joint and GJ is the LVDT placed in mid of span with Gerber joints. Locations of LVDTs are the same for both test setups i.e. midspans and Gerber joint location. These LVDTs measure global deflection, but for test setup-1 additional LVDTs were used at overlap end to measure gap opening and closing between profiles. This gap measurement is necessary to know if modified Gerber joint behaves as desired i.e. hinge in elastic phase and continuous in the post-elastic phase.

Table 3: Description of LVDTs

Gauge No.	Gauge Location	Designation for Test Setup-1	Designation for Test Setup-2
1	Midspan	T1-0.85/1-500-MS	T2-0.85/1-100-MS
2	Gap b/w profiles	T1-0.85/1-500-Gap	-
3	Gerber Joint	T1-0.85/1-500-GJ	T2-0.85/1-100-GJ
4	Gerber Mid span	T1-0.85/1-500-GM	T2-0.85/1-100-GM

4. Results and Discussions:

4.1 Elastic moment capacity comparison of test and design rules:

A total of four experiments were conducted; two tests on each profile thickness with two different overlap lengths. Experimental moments were calculated using elastic bending moment equations by considering beam as continuous for test setup-1 and assuming an internal hinge at Gerber joint location for test setup-2. Weights of the I-section beam, hollow steel sections and timber blocks were included in the calculation of applied loads. Elastic moment resistances as well as the failure modes of the section over internal support have been compared with predicted capacities and modes obtained from EWM in Euro codes [8,9] and DSM [12]. Since the sheeting profiles were prevented against lateral-torsional buckling, local and distortional modes were controlling factors for member capacity.

4.1.1 Effective Width Method:

EWM is used by Eurocodes [8,9] for the design of CFS sections with the basic idea of reducing the cross-sectional area. To account for local buckling, the width of plate elements adjacent to stiffeners is reduced. For distortional buckling (flexural buckling of the stiffener itself), an iterative procedure is adopted to calculate the reduction factor which considers elastic buckling stress of stiffeners, flexural stiffness of adjacent plate elements and material yield strength. Once the reduced cross-sectional area is obtained, critical elastic local buckling stress ($\sigma_{cr,\,l}$) and critical elastic distortional buckling stress ($\sigma_{cr,\,d}$) are calculated. For a plate under uniform compression, critical elastic local buckling ($\sigma_{cr,\,l}$) stress, critical distortional buckling stress for flanges with one intermediate stiffener ($\sigma_{cr,s}$) and critical distortional buckling stress for webs with up-to two intermediate stiffeners ($\sigma_{cr,sa}$) are calculated by Eqs. 1, 2 and 3 respectively.

$$\sigma_{(cr,l)} = \frac{k_\sigma \lambda^2}{12(1-v)}\left(\frac{t_n}{b_n}\right)^2 \tag{1}$$

$$\sigma_{(cr,s)} = \frac{4.2 k_w E}{A_s}\sqrt{\frac{I_s t^3}{4{b_p}^2\left(2b_p + 3b_s\right)}} \tag{2}$$

$$\sigma_{(cr,sa)} = \frac{1.05 k_f E\sqrt{I_s t^3 s_1}}{A_{sa} s_2\left(s_1 - s_2\right)} \tag{3}$$

Interaction between flexural buckling of both the flange and web stiffeners are included by modified elastic critical stress ($\sigma_{cr,\ d,\ mod}$) calculated by Eq. 4.

$$\sigma_{(cr,\mathrm{mod})} = \frac{\sigma_{cr,s}}{\sqrt[4]{1+\left[\beta_s \frac{\sigma_{cr,s}}{\sigma_{cr,sa}}\right]}} \qquad (4)$$

Calculated critical buckling stresses and moment capacities for trapezoidal sheeting profile using EWM are presented in Table 4. The resistance of the web to resist shear was neglected as the support cleat is arranged to prevent the distortion of the web. As per calculations, critical distortional buckling stress is lowest for web stiffener closer to compression flange ($\sigma_{cr,sa}$) and highest for the compression flange stiffener ($\sigma_{cr,s}$). A comparison of predicted negative capacities (M^-) with experimental capacities showed that EWM predictions were conservative by 29% and 27% for 0.85 mm and 1 mm profiles respectively.

Table 4: Elastic load capacity comparison with EWM

Profile Thickness	$\sigma_{cr,s}$ (MPa)	$\sigma_{cr,sa}$ (MPa)	$\sigma_{cr,d,mod}$ (MPa)	W_{eff} (mm^3)	M^- (EWM) (kNm)	Test Failure Moment (kNm)	% Difference
0.85	1018	194.40	280	20553	8.63	12.24	29%
1	1193.78	219.31	312.24	26666	11.20	15.38	27%

4.1.2 Direct Strength Method (DSM):

The direct strength method (DSM) is a semi-analytical approach using a combination of numerical analysis and design formulas. Initially, linear elastic stability analysis is carried out by using specially developed computational finite strip analysis program CUFSM [32]. A single trapezoidal sheeting profile with simply supported boundary conditions and bottom flange in compression was modelled in CUFSM. For profile modelling, coordinates of each node related to the mid-line of cross-section were introduced in CUFSM which creates plate elements between these nodes. Division of elements was refined near the corners and a minimum of four elements per plate in compression was used to obtain accurate results. The manufacturer recommended modulus of elasticity E=210GPa and, Poisson's ratio 0.3 and shear modulus of elasticity 81 GPa were used. Stress profiles related to yield stress of 420 MPa were generated in the same program and wavelengths were selected so as to include local as well as distortional buckling modes of profile. Buckling modes and corresponding load reduction factors for trapezoidal sheeting profiles with the bottom flange in compression (internal support condition) are shown in Figure 7. Elastic buckling modes for both the profile thicknesses were the same and global buckling was ignored in calculations as it is not encountered in actual scenarios.

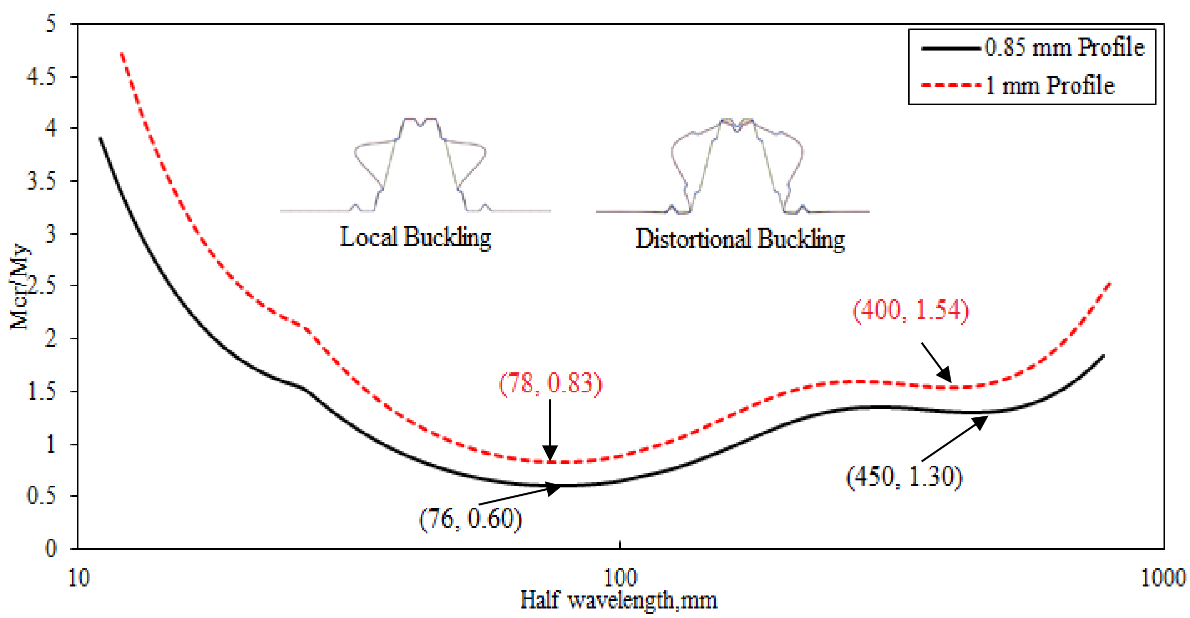

Figure 7: Finite strip analysis results from CUFSM

Based on elastic instability modes i.e. local, distortional, global buckling modes and corresponding strength reduction factors, the strength of CFS sections can be calculated by using direct formulas given in chapter F of AISI S100-16 specifications [12]. The nominal strength of members including the potential of the inelastic reserve is minimum of global, local and distortional buckling strength calculated by Eqs. 5 through 10.

$$M_n = \min\left(M_{ng}, M_{nlg}, M_d\right) \tag{5}$$

$$M_{ng} = \begin{cases} M_{cre} & \text{if } M_{cre} < 0.56M_y \\ \dfrac{10}{9}M_y\left(1-\dfrac{10M_y}{3.6M_{cre}}\right) & \text{if } 2.78M_y \geq M_{cre} \geq 0.56M_y \\ M_y & \text{if } M_{cre} > 2.78M_y \end{cases} \tag{6}$$

$$M_{nl} = \begin{cases} M_{ne} & \text{if } \lambda_l \leq 0.776 \\ \left(1-0.15\left(\dfrac{M_{crl}}{M_{ne}}\right)^{0.4}\right)\left(\dfrac{M_{crl}}{M_{ne}}\right)^{0.4} M_{ne} & \text{if } \lambda_l > 0.776 \end{cases} \tag{7}$$

where $\lambda_l = \sqrt{\dfrac{M_{ne}}{M_{crl}}}$ (8)

$$M_{nd} = \begin{cases} M_y & \text{if } \lambda_d \leq 0.673 \\ \left(1-0.22\left(\dfrac{M_{crd}}{M_y}\right)^{0.5}\right)\left(\dfrac{M_{crd}}{M_y}\right)^{0.5} M_y & \text{if } \lambda_d > 0.673 \end{cases} \tag{9}$$

Where $\lambda_d = \sqrt{\dfrac{M_y}{M_{crd}}}$ (10)

Yield moment (M_y), reduction factors for local (M_{crl}/M_y) and distortional (M_{crd}/M_y) buckling, factored moment capacity (ΦM_n) and experimental moment capacities are presented in Table 5.

DSM predictions were found to be in good agreement with experimental moment capacities as the difference between two values is insignificant.

Table 5: Elastic load capacity comparison with DSM predictions

Profile Thickness	M_y (kN-m)	$M_{cr\ell}/M_y$ (MPa)	M_{crd}/M_y (MPa)	ΦM_n (kNm)	Test Failure Moment (kNm)	% Difference
0.85	19.74	0.6	1.3	11.91	12.24	2.6%
1	23.22	0.83	1.54	15.38	15.38	0%

The conservative nature of EWM predictions for this profile conforms with previous studies on the limitations of EWM for complex cross-sectional shapes. EWM is a semi-empirical approach that breaks down the CFS section into plate elements and stiffeners at fold point locations. It then follows a cumbersome process of calculating critical buckling stresses and effective sections of each plate element and stiffener with a reduction factor calculated separately for these elements. In this whole process, the interaction between plate elements, interelement equilibrium and compatibility is ignored which leads to inaccurate prediction of strength and failure modes, especially the dominant distortional buckling mode for complex sections with intermediate stiffeners. In opposition to that, DSM is a combination of computational tools and design equations and considers gross section properties to conduct linear elastic buckling analysis of any cross-sectional shape and critical buckling load calculation. In DSM, the reduction factor is applied to complete cross-section and compatibility between plate elements is maintained. The constrained finite strip method in DSM facilitates the easier, understandable and economical calculation of relevant buckling modes and strength reduction factors that are used in simplified design equations for accurate calculation of member’s capacity.

4.2 Moment redistribution and load capacity comparison of single span and double span:

Due to the post-elastic strength of CFS profiles and resulting moment redistribution, the ultimate load capacity of such profiles for multi-span applications can be higher than predicted capacities which are based on elastic resistance of single-span profiles. Due to relatively high slenderness of CFS profiles, redistribution of moments in the post-elastic phase occurs with reduced bending resistance of section over internal support (Figure 1a). Ideal redistribution of moments is achieved when the section in mid-span reaches its elastic moment capacity. This post-elastic redistribution of moments depends on the shape and thickness of CFS profiles.

Previous tests on shallow decking profiles summarized by Lawson and Popo-Ola [19] showed that load-capacity of multi-span CFS profiles can be derived by replacing the section over internal support with a plastic hinge with reduced elastic negative bending resistance. Ultimate load capacity for a two-span test with four load points on span can be determined by Eq. 11.

$$q_{test} = \frac{L^2}{8}\left(M^+ + 0.38kM^-\right) \tag{11}$$

Where q_{test} is equivalent uniform loading at failure, L is the length of each span, M^+ is elastic bending resistance in mid-span, M^- is elastic bending resistance of section over internal support and k is residual moment strength factor which is the ratio of reduced elastic bending resistance to full elastic bending resistance of section over internal support.

The value of k can be determined by the method described in CIRIA technical note [25] which was also used by previous studies on multi-span purlins [20] and continuous decking [19, 26]. This is a graphical method where k is obtained by overlapping experimentally obtained moment-rotation curve with conventional beam-line. The moment-rotation curve under negative bending is obtained by conducting a three-point bending test on an inverted decking profile with a span length of 0.4xL replicating support reaction and moment at internal support. For continuous decking understudy, the moment-rotation relationship was obtained from test setup-2. Since the Gerber joint in this test setup does not transfer moments in the post-elastic phase, the location of this Gerber joint acts as a point of contra-flexure even in the post-elastic phase. The deflection was measured at Gerber joint location (GJ) and moments calculated as per moment equations. The post elastic component of deflection was calculated by subtracting elastic deflection from total deflection at each load level. For CFS profiles, it is considered that deformation is concentrated at load point only, therefore, post-elastic rotation is obtained by dividing deflection by distance between internal support and LVDT location. For beam line, section over internal support in multi-span system is replaced by an equivalent spring with stiffness ranging from zero for simply supported condition to full stiffness. The y-axis of beam line is equal to moment at internal support when a multi-span beam is subject to uniform loading. The x-axis is the rotation of this spring with zero spring stiffness making the beam as simply supported. The position of beam line varies according to applied load and the actual value of load is the failure load of multi-span profile obtained by iteration.

Values of reduced bending resistance (k) obtained by CIRIA method, ultimate load capacity and experimental load capacity of multi-span profile for test setup-1 are summarized in Table 6: Single and double span load capacities for trapezoidal sheeting. The manufacturer recommended a single-span failure load is used and the double span failure load (Table 1) was calculated by using Eq. 11 and experimental value was obtained from test setup-1.

Table 6: Single and double span load capacities for trapezoidal sheeting

Profile Thickness (mm)	k	Single Span failure load - Elastic (kN)	Double Span failure load – Eq. 11 (kN)	Double span failure load - experimental (kN)	% Load increase over elastic design
0.85	0.76	28.29	28.82	30.31	7.14
1	0.81	39.07	41.06	42.5	8.80

From the results in Table 6, the percentage load increase for double span profile as compared to single-span elastic capacity is 7.14% and 8.80% for 0.85 mm and 1 mm profile respectively. The percentage load increase for multi-span profile increases with profile thickness, which is due to higher post-elastic strength for lower slenderness.

It is worth mentioning that this percentage load increase for highly stiffened trapezoidal sheeting is lower than previous studies, whereas, the negative residual moment strength factor (k) is higher. This ultimate load capacity for the double span system is low due to the lower moment capacity of the section in mid-span (M^+) which doesn't allow for high redistribution of moments. This ultimate load can be higher for other CFS profiles with comparatively higher mid-span section capacities. However, it can be concluded from this study and previous studies on decking profiles that redistribution of moments in the post-elastic phase improves load capacity and economy in design for such profiles.

4.3 Load-Displacement Relationship:

The typical load-displacement curve of a single span CFS section in bending is shown in Figure 1a. As these types of cross-sections are classified as class 4 or slender sections, their typical load-displacement curve looks like a backbone curve with reduced load capacity in the post-elastic phase. The load-displacement curves from this experimental program as a function of vertical displacement at mid-span for test setup-1 and test setup-2 are shown in Figure 8a&b. The structural behaviour of tested beams in the elastic phase (loading stage and elastic load capacity) is identical for all thicknesses and overlap lengths. Since the section over internal support is subjected to higher moments, therefore, failure is initiated at this section through local buckling of web plate adjacent to compression flange for both profile thicknesses and test setups. Loss of cross-sectional stiffness after this initiation of bucking was gradual as exhibited in the load-displacement curve which shows a linear response till the elastic limit. At this stage, the neutral axis starts shifting towards top flange and this shift depends on profile thickness. For 0.85mm thick profile, this shift was quite low (Figure 9a&c) as compared to the 1mm profile where buckling was observed in top stiffener also (Figure 9b&d). This indicates a greater shift of neutral axis in the post-elastic phase and consequently greater inelastic strength reserve for the thicker (less slender) profile.

Another important observation in load-deflection behaviour is the effect of the overlap length of the modified Gerber joint on the post-elastic behaviour of the multi-span system. Profiles with 500mm overlap length can sustain their elastic load capacity under post-elastic deflections (Figure 8a) compared to profiles with 100mm overlap length (Figure 8b). This indicates continuity provided by the modified Gerber joint in the post-elastic range. This continuity allows redistribution of moments in the post-elastic phase which was the basic design intention for the modified Gerber joint. Since the moments were redistributed in test setup-1, the ultimate collapse occurred when the section in the mid-span reached its elastic moment capacity (Figure 10a). On the other hand, the Gerber joint in test setup-2 was unable to transfer moments in the post-elastic range, thus the system collapsed due to the failure of this Gerber joint (Figure 10b).

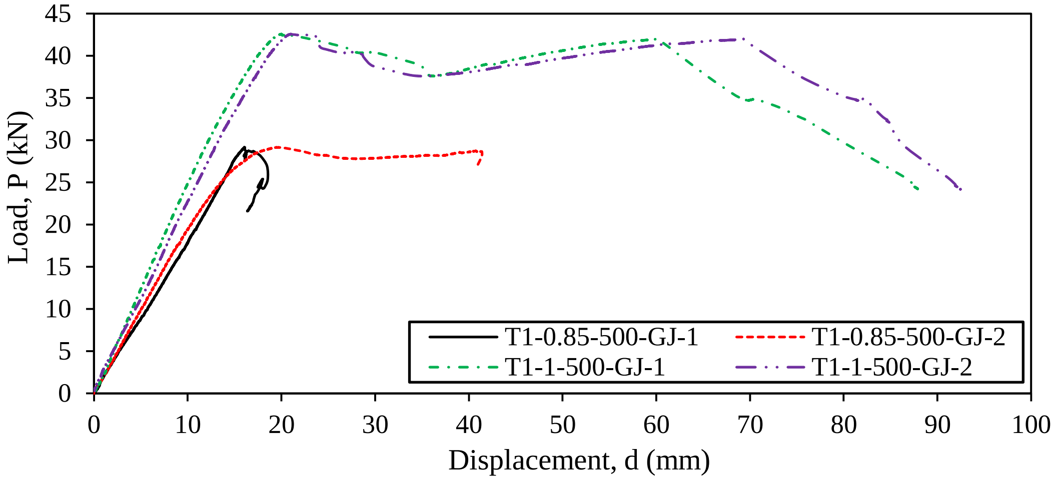

(a)

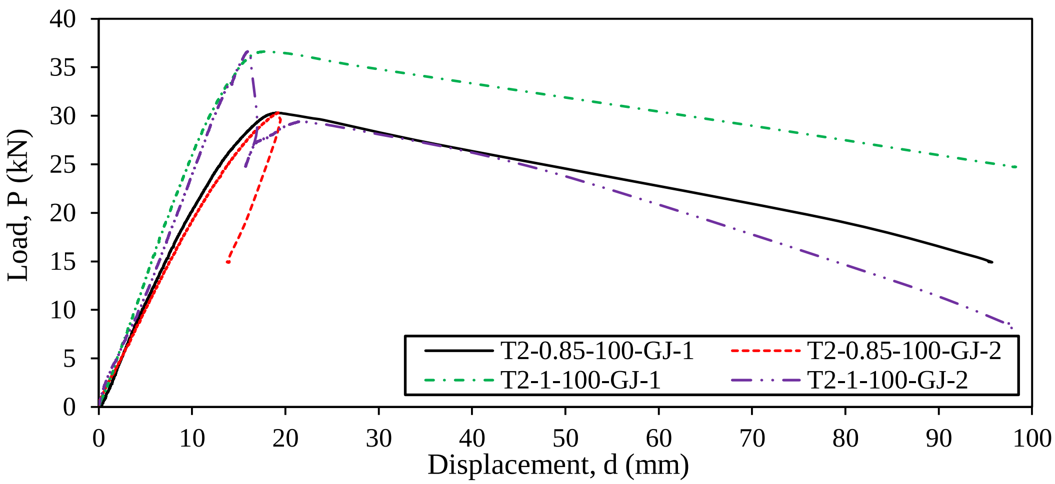

(b)

Figure 8: Load-Displacement relationship of both profiles (a) Test setup 1 (b) Test Setup 2

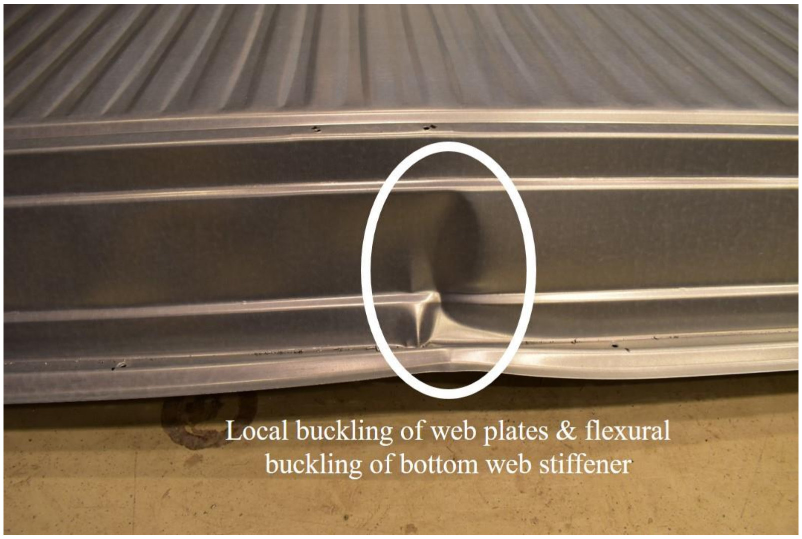
Local buckling of web plates & flexural
buckling of bottom web stiffener

(a)

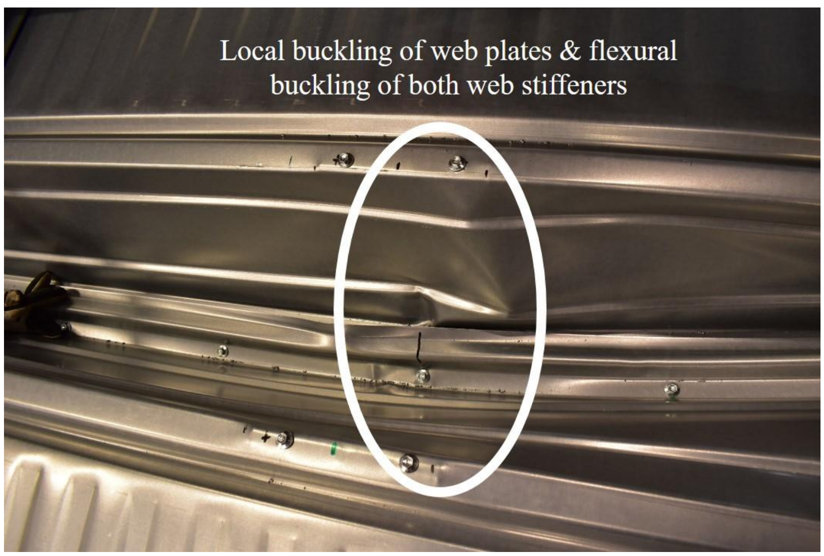
Local buckling of web plates & flexural
buckling of both web stiffeners

(b)

(c)

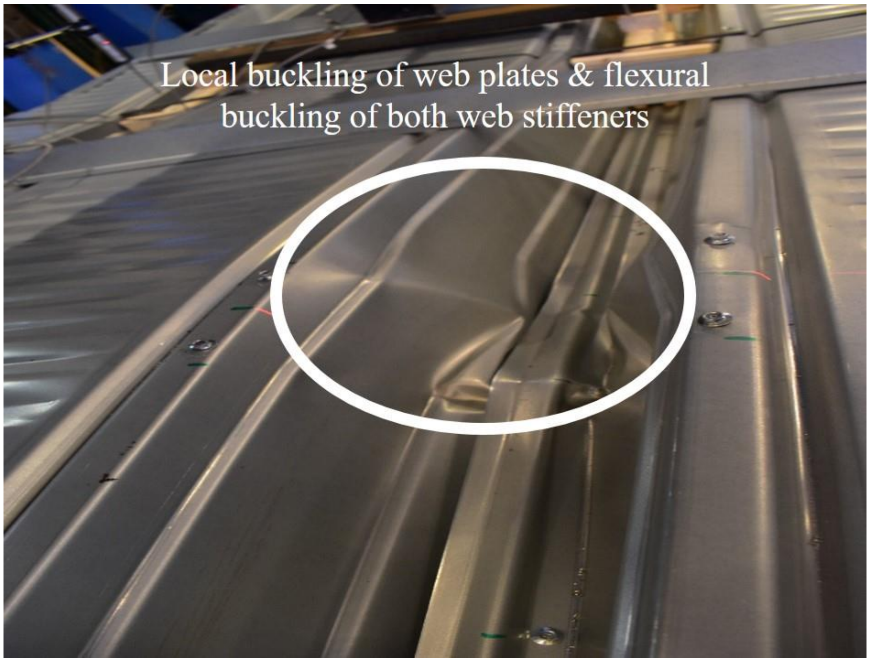

(d)

Figure 9: Failure modes at internal support (a) 0.85 mm –Setup 1 (b) 1 mm –Setup 1 (c) 0.85 mm –Setup 2 (d) 1 mm –Setup 2

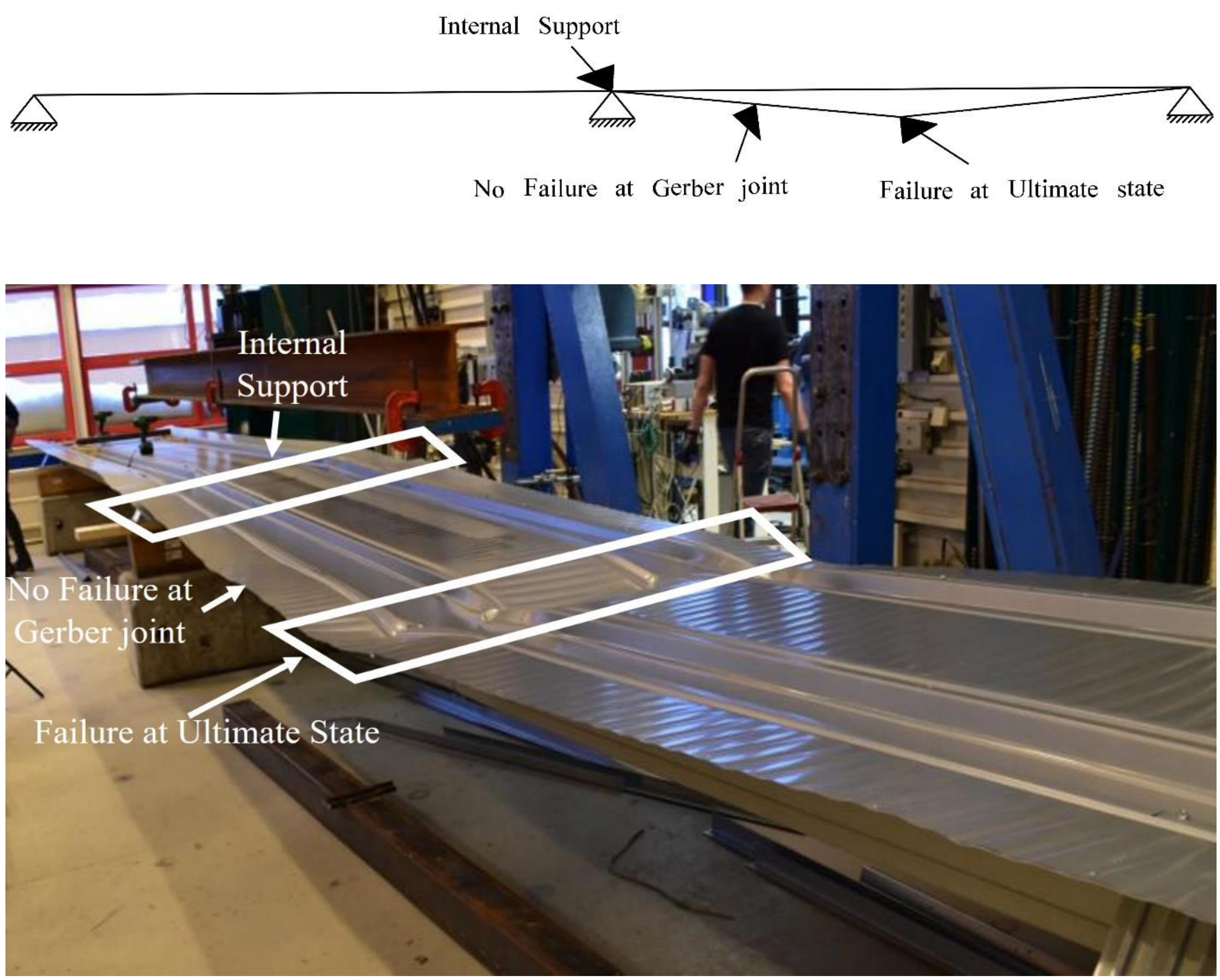
Internal Support
No Failure at Gerber joint
Failure at Ultimate state
Internal
Support
No Failure at
Gerber joint
Failure at Ultimate State

(a)

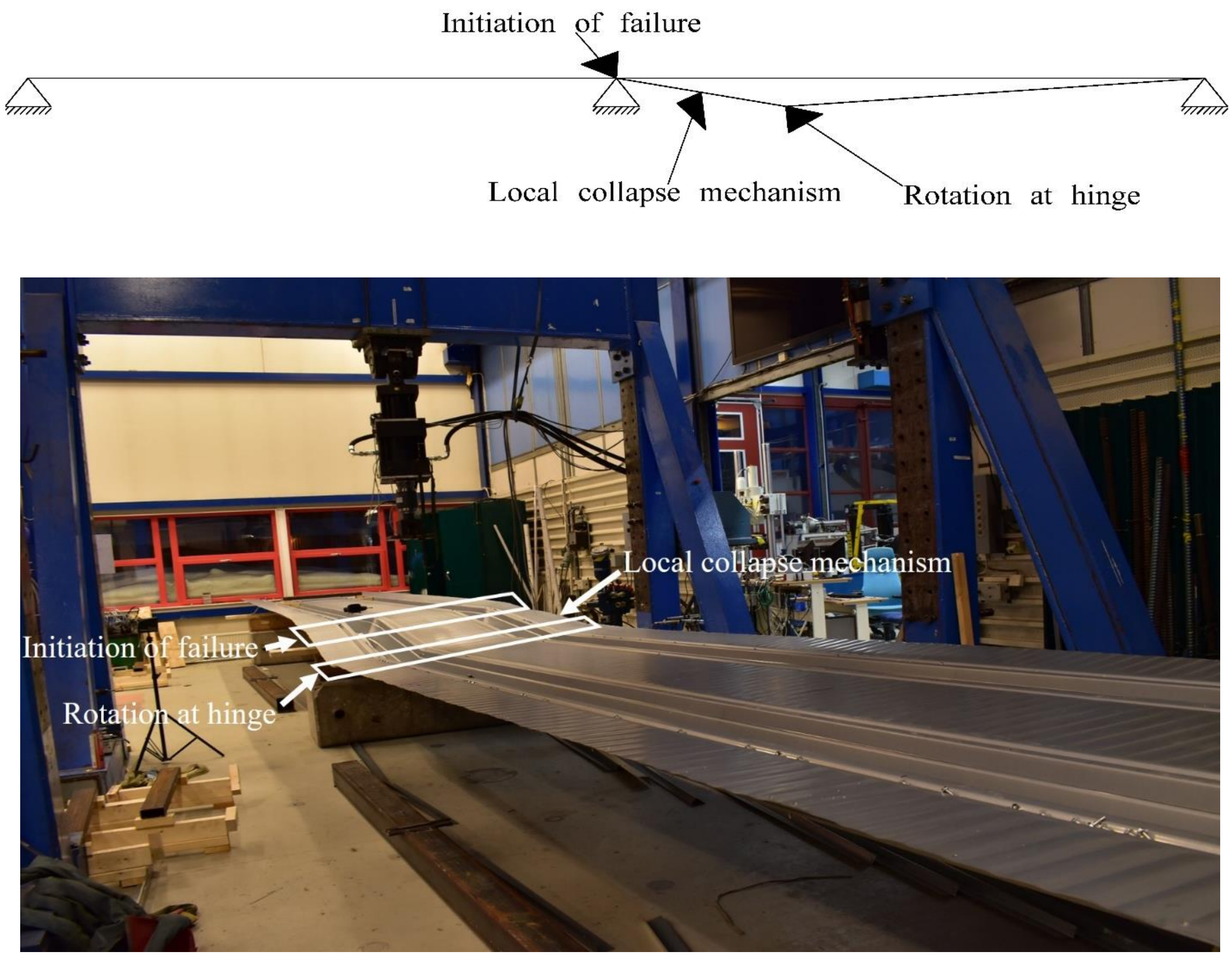

(b)

Figure 10: Comparison of collapse mechanisms for 1 mm profile (a) test setup 1 (b) test setup 2

4.4 Behaviour of Modified Gerber Joint:

Gerber joint has been modified by increasing the overlap length to 500mm and transferring the position of screws to far end from internal support. The modified behaviour was studied by comparing the results of test setup 1 (500 mm overlap) and test setup 2 (100 mm overlap). The intention behind the design of the modified Gerber joint that it behaves as a hinge in the elastic phase and as continuous in the post-elastic phase (Figure 4) was confirmed by measuring the gap between two profiles (Figure 11).

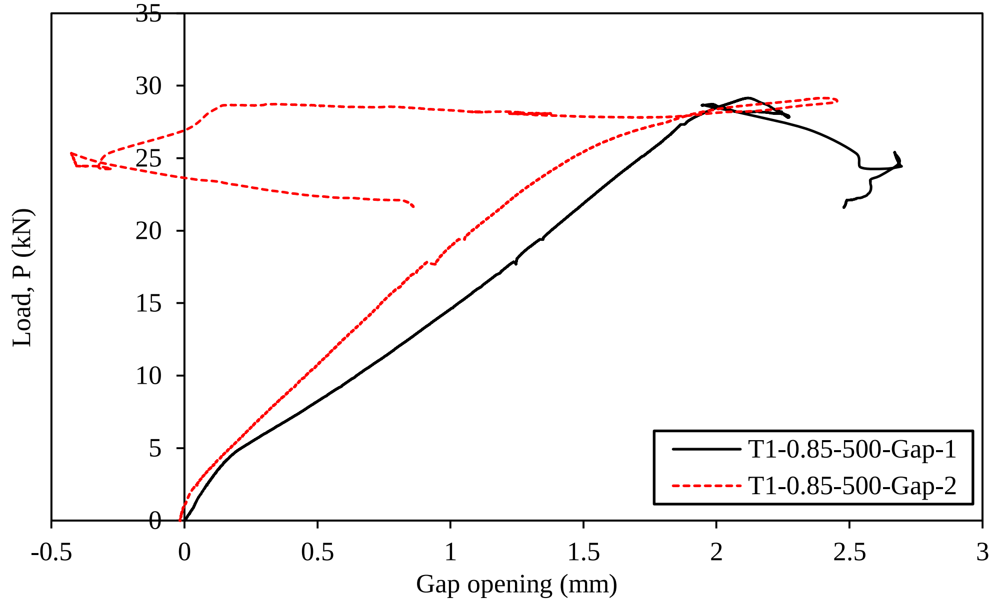

(a)

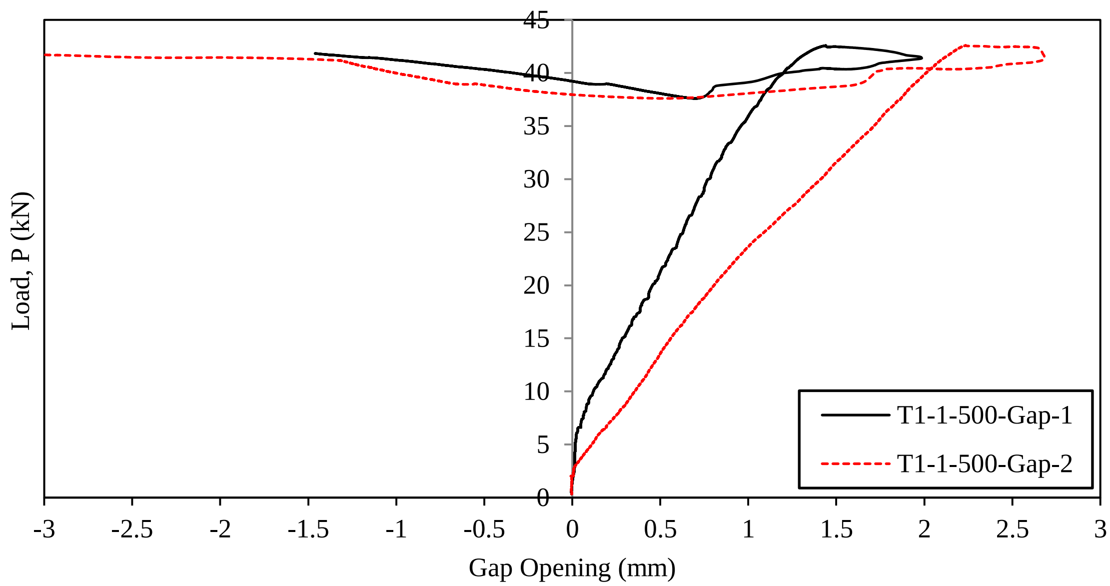

(b)

Figure 11: Load versus opening and closing of the gap in test setup 1 for (a) 0.85 mm (b) 1 mm thick profile.

As the section over internal support is fully stiff before initiation of buckling, rotation of profiles around screws in the overlap is such that the gap between profiles opens. As the gap opens, the only shear force is transferred through the screws and the joint behaves as a hinge. As the section over internal support loses stiffness after initiation of buckling, the gap between profiles closes and continuity is attained due to which joint starts transferring moments. In normal loading conditions, this profile is used with or without insulation and opening of the gap is not affected. Also, the gap opening is very small i.e. 2.70 mm to cause any serviceability problem.

The difference in the behaviour between two setups with different overlap lengths is significant in the post-elastic phase of section over internal support. As this section fails, it loses stiffness and cannot retain its full moment capacity (M^-) due to which the system tends to re-distribute moments until the section in the mid-span reaches its moment capacity (M^+). However, the rotation capacity of section over internal support and continuity of Gerber hinge is pre-requisite for this moment re-distribution, which has been investigated in this experimental part through (i) comparison of the mid-span deflections of both test setups and (ii) comparison of the failure mode between two test setups.

A comparison of load-deflection curves as a function of mid-span deflection is presented in Figure 12. In this graph, deflections of mid-span having Gerber joint are compared between two profiles with the same thickness but different overlap lengths. It can be seen that the setup with longer overlap length can sustain more loads for the same magnitude of deflection in the post-elastic phase, indicating the continuity attained by this longer overlap. In this scenario, the capacity of the section in the mid-span can be fully utilized which was also observed in the ultimate collapse of the system. The comparison of failure modes of both test setups is shown in Figure 10. It can be observed that shorter overlap is unable to transfer moments and multi-span profile cannot sustain higher loads in the post-elastic phase and the ultimate state is reached by the collapse of the section over internal support or failure of Gerber joint.

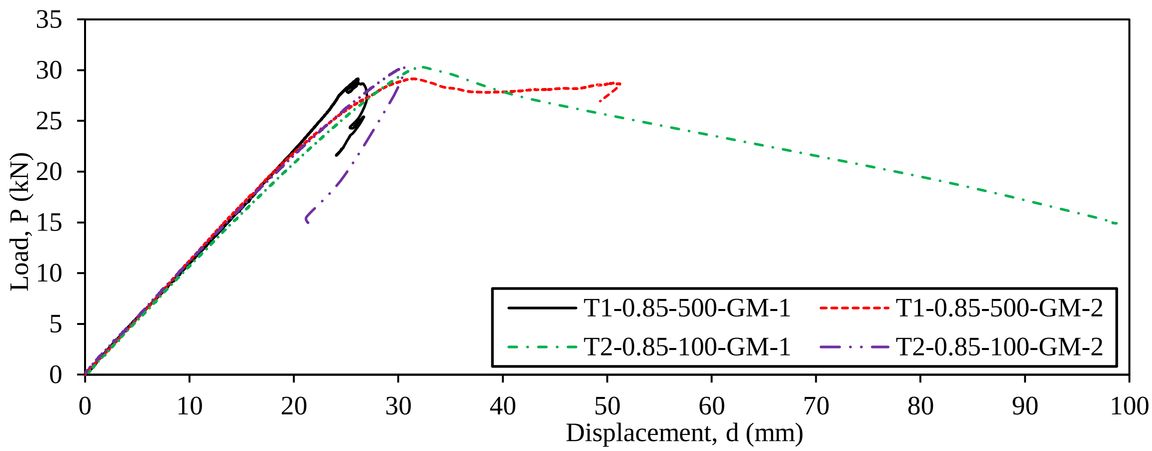

(a)

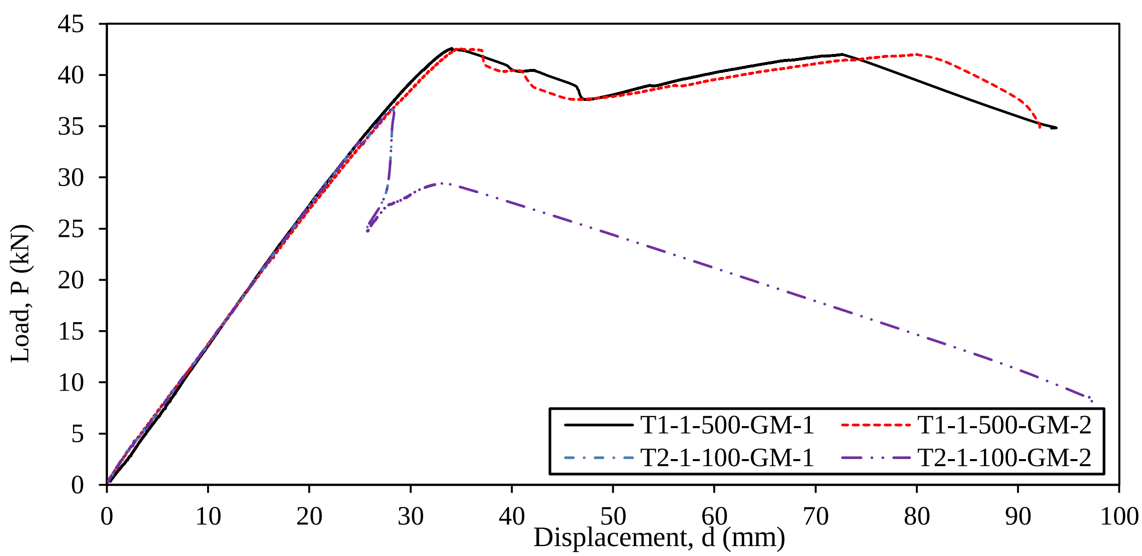

(b)

Figure 12: Mid-span deflection comparison between test setup 1 and 2 for (a) 0.85 mm (b) 1 mm thick profile

5. Conclusions:

Full-scale experiments were conducted on double-span CFS third-generation trapezoidal sheeting profiles. For effective utilization of profile capacity, a special type of cantilever drop-in system known as Gerber joint was used for this profile which proved to be inadequate for accidental and uneven distribution of loads. Design of this Gerber joint has been modified in this research program and experiments were conducted on two types of test setups with 0.85 mm and 1 mm thick sheeting profile i.e. test setup-1 with modified Gerber joint and test setup-2 replicating previous Gerber joint. Results of full-scale experiments have been used to compare experimental elastic capacities and failure modes of section over internal support with Eurocode and DSM predictions, detailed study on inelastic behaviour of multi-span profile, evaluation of moment redistribution and ultimate load capacity and feasibility of modified Gerber joint has also been investigated by comparing results with previous Gerber joint. Following conclusions were drawn:

- Eurocode design predictions based on effective width method (EWM) were found to be conservative and inadequate to predict failure modes for highly stiffened trapezoidal sheeting profile with intermediate stiffeners. Design predictions of Euro codes were conservative by 29% and 27% for 0.85 mm and 1 mm thick profile respectively. In opposition to that, AISI predictions based on direct strength method (DSM) using a combination of easy to use computational tools and design equations predicted the capacities and failure modes accurately. Since DSM maintains equilibrium between elements, uses gross section properties and efficient tools in terms of time and accuracy, therefore, it is recommended to use DSM for strength calculation of complex CFS sections.

- For a multi-span profile, it was found that moment redistribution can further increase the load capacity of CFS members as compared to predicted capacities based on the elastic design of single-span profiles. For multi-span CFS trapezoidal sheeting profile understudy, residual moment capacity ratios of 0.76 and 0.81 in the post-elastic range allowed for 7.14% and 8.80% increase in ultimate load capacity for 0.85 mm and 1 mm thick profiles respectively. Consideration of moment redistribution for multi-span CFS profiles in the design phase can yield enhanced load capacity and economical results.
- The main conclusions of these experimental tests are for multi-span CFS profiles with Gerber joints. The design of Gerber joint was modified in this study by increasing overlap length to 500 mm from 200 mm and connecting the profiles at one end compared to connection in the center. This behaviour of the joint was verified by observing the opening and closing of the gap and comparing the failure modes of two different test setups with different overlap lengths. Since the service load of this profile is a self-weight or additional load of insulation in some cases, gap opening and closing are not affected by these loads. Also, the opening of the gap is so small to cause any serviceability issues. Thus, the Gerber joint is feasible in practice and can yield economical solutions under service loads and safer solutions in accidental loads as compared to the previous design which was unable to carry moments under accidental loads.

Acknowledgments:

The authors gratefully acknowledge Luleå University of Technology for testing facilities and guidance and CFS profile manufacturer Lindab International for providing testing materials.

References:

[1] Laím L, Rodrigues JPC, Silva LS da. Experimental and numerical analysis on the structural

behaviour of cold-formed steel beams. Thin Walled Struct 2013;72:1–13. doi:10.1016/j.tws.2013.06.008.

[2] Cheng Y, Schafer BW. Local buckling tests on cold-formed steel beams. J Struct Eng 2003;129:1596–606. doi:10.1061/(ASCE)0733-9445(2003)129:12(1596).

[3] Yu C, Schafer BW. Simulation of cold-formed steel beams in local and distortional buckling with applications to the direct strength method. J Constr Steel Res 2007;63:581–90. doi:10.1016/j.jcsr.2006.07.008.

[4] Wang H, Zhang Y. Experimental and numerical investigation on cold-formed steel C-section flexural members. J Constr Steel Res 2009;65:1225–35. doi:10.1016/j.jcsr.2008.08.007.

[5] Dinis PB, Camotim D. Local/distortional mode interaction in cold-formed steel lipped channel beams. Thin Walled Struct 2010;48:771–85. doi:10.1016/j.tws.2010.01.005.

[6] Haidarali MR, Nethercot DA. Local and distortional buckling of cold-formed steel beams with both edge and intermediate stiffeners in their compression flanges. Thin Walled Struct 2012;54:106–12. doi:10.1016/j.tws.2012.02.013.

[7] Franco JMS, Batista EDM. Buckling behavior and strength of thin-walled stiffened trapezoidal CFS under flexural bending. Thin-Walled Struct 2017;117:268–81. doi:10.1016/j.tws.2016.11.027.

[8] EN 1993-1-5: Eurocode 3: Design of steel structures - Part 1.5: Plated structural elements. vol. 5. 2003.

[9] EN 1993-1-3 (2006): Eurocode 3: Design of steel structures - Part 1-3: General rules -

Supplementary rules for cold-formed members and sheeting. vol. 3. 2011.

[10] Manual A. AISI Manual cold-formed steel design 2002 edition 2003.

[11] American Iron and Steel Institute (AISI) S100. Supplement no. 2 to the North American specification for the design of cold-formed steel structural members 2007 edition. Aisi S100 2010.

[12] AISI S100-16. North American specification steel structural members. North Am Specif Steel Struct Members 2016:78.

[13] Schafer BW. Advances in the direct strength method of cold-formed steel design. Thin-Walled Struct 2019;140:533–41. doi:10.1016/j.tws.2019.03.001.

[14] Schafer BW. Review : The direct strength method of cold-formed steel member design. J Constr Steel Res 2008;64:766–78. doi:10.1016/j.jcsr.2008.01.022.

[15] Yener M, Pekoz T. Partial stress redistribution in cold-formed steel. J Struct Eng 1985;111:1169–86.

[16] Reck HP, Winter G, Pekoz T. Inelastic strength of cold-formed steel beams. J Struct Div 1975;101:2193–203.

[17] Maduliat S, Bambach MR, Zhao XL. Inelastic behaviour and design of cold-formed channel sections in bending. Thin Walled Struct 2012;51:158–66. doi:10.1016/j.tws.2011.10.011.

[18] Laím L, Rodrigues JPC, Craveiro HD. Flexural behaviour of beams made of cold-formed steel sigma-shaped sections at ambient and fire conditions. Thin Walled Struct 2015;87:53–65. doi:10.1016/j.tws.2014.11.004.

[19] Lawson RM, Popo-Ola S. Load capacity of continuous decking based on small-scale tests. Thin-Walled Struct 2013;69:79–90. doi:10.1016/j.tws.2013.03.011.

[20] Liu Q, Yang J, Long Yuan L. Pseudo-plastic moment resistance of continuous beams with cold-formed sigma sections at internal supports: A numerical study. Eng Struct 2011;33:947–57. doi:10.1016/j.tws.2011.08.007.

[21] Hui C, Gardner L, Nethercot DA. Moment redistribution in cold-formed steel continuous beams. Thin-Walled Struct 2016;98:465–77. doi:10.1016/j.tws.2015.10.009.

[22] Unger B. Ein Betrag zur Ermittlung der Traglast von querbelastaten Durchlauf- tragern mit dunnwandigen Querschnitt. 'A contribution to the determination of the service load for thin walled continuous beams.' vol. 1. 1973.

[23] Leach P. Tests on profiled steel sheeting for composite floors. Manchester: 1984.

[24] Luure P, Crisinel M. Redistribution of moments at the interior support of cold formed sheeting. Lausanne: 1993.

[25] Bryan E, Leach P. Design of profiled sheeting as permanent formwork. London: 1984.

[26] Davies JM, Jiang C. Design procedures for profiled metal sheeting and decking. Thin-Walled Struct 1997;27:43–53.

[27] Herbert L, Bill J. Cantilever and suspended span roof framing system. J Archit Engieering 2000;6:35–8.

[28] Sjolander J, Tiderman E. Gerber splicing in thin steel sheeting of roofs a study of rotational stiffness in the joint. Chalmers University of Technology, Sweden, 2016.

[29] Johansson C-J, Lidgren C, Nilsson C, Crocetti R. Takras vintrarna 2009/2010 och 2010/2011 Orsaker och förslag till åtgärder, Roofs Collapsed in winters 2009/2010 and 2010/2011: reasons and suggestions for action. 2011.

[30] Strömberg J, Veljkovic M. Utredning av skador på Fotbollshall i Skellefteå, Investigation of damage of football hall in Skellefteå. Luleå: 2010.

[31] Strömberg J, Veljkovic M. Utredning av takras B-hallen, Luleå, 2010, Investigation of roof collapse of Hall-B, Luleå. Luleå: 2010.

[32] Schafer BW, Ádány S. Buckling analysis of cold-formed steel members using CUFSM: Conventional and constrained finite strip methods. Eighteenth Int Spec Conf Cold-Formed Steel Struct Recent Res Dev Cold-Formed Steel Des Constr 2006;2006:39–54.